drones

MDPI

Article

Aeroacoustic Source Mechanisms of Fixed-Wing VTOL Configuration at Takeoff Hover †

Paruchuri Chaitanya [1,*], Thomas Corbishley [1], Sergi Palleja-Cabre [1], Minki Cho [1], Amin Karimian [1], Phillip Joseph [1], Deepak C. Akiwate [2], Oliver Westcott [3] and Swathi Krishna [3]

[1] Institute of Sound and Vibration Research, University of Southampton, Southampton SO17 1BJ, UK; t.d.corbishley@soton.ac.uk (T.C.); s.palleja-cabre@soton.ac.uk (S.P.-C.); m.cho@soton.ac.uk (M.C.); a.karimian@soton.ac.uk (A.K.); pfj@isvr.soton.ac.uk (P.J.)
[2] Acoustics Research Centre, University of Salford, 43 Crescent, Salford M5 4WT, UK; d.c.akiwate@salford.ac.uk
[3] Department of Aeronautics & Astronautics, University of Southampton, Southampton SO17 1BJ, UK; o.c.s.westcott@soton.ac.uk (O.W.); s.b.krishna@soton.ac.uk (S.K.)
* Correspondence: c.c.paruchuri@soton.ac.uk
† This work extends the conference version of the paper presented in Chaitanya, P.; Cho, M.; Palleja-Cabre, S.; Akiwate, D.C.; Joseph, P.; Westcott, O.; Ferraro, M. Aeroacoustics source mechanisms of fixed-wing VTOL configuration. In Proceedings of the AIAA AVIATION 2023 Forum, San Diego, CA, USA, 12–16 June 2023.

Highlights

What are the main findings?

- The study identifies two dominant noise generation mechanisms in unmanned fixed-wing VTOL propeller–wing configurations at takeoff: (1) interference between direct and image sources due to acoustic reflections from the wing, and (2) unsteady blade loading caused by azimuthal flow variations as the propeller blades pass over the wing when overlaps.
- Analytical modelling based on Goldstein's formulation and inflow-distortion theory validates that unsteady lift due to proximity effects is the primary noise source under takeoff hover conditions.

What are the implications of the main findings?

- The study demonstrates that close propeller–wing spacing in VTOL aircraft can significantly amplify tonal and broadband noise, emphasising the importance of installation geometry in low-noise vehicle design.
- The findings provide guidance for designing quieter unmanned fixed-wing VTOL configurations by optimising propeller–wing separation and overlap to minimise unsteady loading and reflection-driven amplification.

Abstract

This paper presents an experimental and analytical investigation into the dominant noise generation mechanisms of unmanned Fixed-wing Vertical Take-Off and Landing (VTOL) propeller–wing configurations during takeoff. This paper reports the velocity measurements made in the close vicinity of a scale-model propeller adjacent to a flat plate or wing, aimed at understanding and characterising its dominant noise generation mechanisms. This paper identifies two main interaction mechanisms. The first is a purely acoustical phenomenon whereby the wing acts as an image source causing strong interference between the direct and image noise sources due to the propeller. The second is a significant noise increase resulting from the unsteady blade loading that occurs when the blade passes over the wing at lower vertical separation distances. Other, more minor noise sources from the propeller and the wing are also discussed in this paper.

Academic Editor: Abdessattar Abdelkefi

Received: 4 October 2025
Revised: 27 November 2025
Accepted: 9 December 2025
Published: 15 December 2025

Citation: Chaitanya, P.; Corbishley, T.; Palleja-Cabre, S.; Cho, M.; Karimian, A.; Joseph, P.; Akiwate, D.C.; Westcott, O.; Krishna, S. Aeroacoustic Source Mechanisms of Fixed-Wing VTOL Configuration at Takeoff Hover. *Drones* **2025**, *9*, 864. https://doi.org/10.3390/drones9120864

Keywords: aeroacoustics; unmanned fixed-wing VTOL; unsteady loading noise

1. Introduction

The growing interest in Urban Air Mobility (UAM) and Unmanned Aircraft Systems (UAS) has boosted research and development of non-conventional aircraft configurations. Unmanned fixed-wing Vertical Take-Off and Landing (VTOL) configurations offer significant advantages over other aircraft for urban operations, such as their potential to provide enhanced speed and range compared to conventional rotorcraft while maintaining the ability to operate from smaller and more constrained spaces [1,2]. However, it is now widely acknowledged that noise is one of the key factors in limiting public acceptance and adoption of these technologies. The integration of the propulsion system with the wing should therefore not be solely based on operational requirements but also account for the potential impact on the acoustic signature of the vehicle.

The noise radiated by propellers in isolation has been extensively studied. However, interactions of the wing and propeller induce source mechanisms that are not yet fully understood. While the aeroacoustic mechanisms of propeller–wing interaction during conventional forward flight have been studied theoretically and experimentally in recent work, new sources are introduced during the transition phases, especially during vertical takeoff, which also alter the balance of existing ones. This lack of understanding presents a significant challenge in predicting and mitigating the noise impact of these vehicles in urban environments, where noise pollution is a major concern [3–6]. The novel arrangement of the propeller wing setup in this study addresses the vertical takeoff condition.

NASA has proposed reference concept vehicles representative of typical configurations currently being adopted in the industry [7]. The fixed-wing architectures can be broadly categorised into (1) Tilt-rotor, (2) Lift+cruise, and (3) Tilt-duct, or a hybrid combination of these configurations. The tilt-rotor configurations have rotors placed on the tips and/or along fixed wings, capable of rotating to provide thrust for both horizontal and vertical flight. Conversely, lift+cruise architectures have separate rotors for vertical takeoff and landing, and cruise conditions. The current work is focused on the characterisation of the noise produced by the interaction between propellers operating near a wing at takeoff conditions, which is of interest both for tilt-rotor and lift+cruise architectures in takeoff conditions. These often comprise a propeller operating above a wing. Not only does the presence of the nearby wing have a substantial effect on the flow in the vicinity of the propeller, but it also reflects the propeller noise, which we shall show has a significant effect on the far-field noise spectrum (referred to here as the 'ground effects').

Lee et al. [8] conducted experiments to study the fluid dynamics of a hovering rotor interacting with a horizontal ground plane and found that the resulting flow field exhibited powerful curvature and straining effects, leading to the development of an unsteady outward flow comprising a wall jet. While the study highlighted various factors affecting the flow field, the noise generated by this flow impinging on the propeller is yet to be investigated. More recently, Hanson et al. [9] investigated experimentally both the performance and noise characteristics of a single propeller hovering over a ground plane. The ground effects were found to increase and reduce the noise depending on the polar angles. The noise increase was attributed to acoustic reflections from the ground plane.

Whilst the tonal and broadband noise from uninstalled propellers has been studied in detail over more than 60 years, comparatively little work has been undertaken on uninstalled propellers in which the propeller operates in a highly non-uniform flow environment. One configuration that has received attention in recent years, which shares

many noise sources in common with the propeller–wing geometry under consideration here, is that of co-axial Contra Rotating Open Rotors (CROR). Detailed studies of the tonal generation by CRORs can be found in [2,10–15].

A recent investigation conducted at NASA [5] studied the aerodynamic and acoustic interactions of inboard propeller–wing configurations. The investigation encompassed systematic variations in the axial separation between the wing leading edge and the propeller disk, as well as the vertical offset relative to the hub. The findings indicate a reduction in inflow distortion effects induced by the wing potential field when increasing the axial separation. The vertical offset was found to play a substantial role in modifying the acoustic directivity at the propeller blade passage frequency (BPF).

Recent analytical investigations have been performed to study the installation effects in tonal noise for configurations where the propeller is installed over the wing and downstream of the wing. In both cases, the propeller plane is perpendicular to the wing platform. Acevedo-Giraldo et al. [16] investigated the case in which the propeller is installed over the wing and partially immersed in the boundary layer. Roger et al. [17] studied the case in which the propeller is installed downstream of the wing and partially immersed in the wing wake. These analytical studies assessed the additional noise sources due to the interaction of the boundary layer or the wing wake with the propeller and the acoustic scattering by the wing trailing edge. Both sources were found to increase with the proximity of the propeller to the trailing edge. The increase in interaction tones was mainly linked to the wake characteristics whereas the steady-loading noise was found to be amplified by edge scattering.

Chen et al. [18] performed aeroacoustic and aerodynamic measurements for a small rotor operating near flat-plate and NACA 0012 wings at low disk loading and Reynolds numbers. Their results show that as the rotor approaches the wing, the deflected rotor wake significantly amplifies low-frequency broadband noise and overall sound pressure levels, while tonal components become less distinguishable. The study highlights the strong influence of wake impingement and rotor–wing spacing on noise generation in small rotorcraft configurations, but does not address propeller–wing overlap effects, which remain largely unexplored.

Chen et al. [19] has expanded understanding of small-rotor/wing interaction by experimentally assessing how steady blowing applied through distributed ports on a flat-plate wing influences both vehicle performance and aero-acoustics. Their study, conducted under low disk-loading hover conditions, demonstrated that appropriate blowing patterns can significantly reduce download force while also modifying the broadband noise associated with the deflected rotor wake. The results highlight the sensitivity of noise and aerodynamic loads to rotor–wing proximity and show that active flow control can play a beneficial role in mitigating adverse rotor-wake effects.

Recent numerical work by Chen et al. [20] examined the aerodynamic and aeroacoustic interactions of a small rotor operating near a generic wing using a transient DES solver in ANSYS Fluent (version 21.2). Their simulations reproduced key experimental trends, including thrust enhancement as the rotor approaches the wing, and identified the role of recirculating wake structures in generating an upwash that modifies rotor loading. While their aeroacoustic predictions captured some features of the far-field sound, limitations in the FW–H formulation prevented accurate representation of flow-induced velocity effects at the microphones. This study highlights the complex aerodynamic mechanisms present even in simplified rotor–wing configurations and further motivates the need for combined experimental and modelling approaches for understanding propeller–wing installation effects. All these works [18–20] provides an important reference for rotor–wing interaction

noise studies, although it does not address propeller–wing overlap noise mechanisms, which remain largely unexplored.

The authors recently explored the 'puller' configuration under hover conditions [6], wherein the propeller is positioned upstream of the wing. It was a predominantly experimental study that showed the sensitivity of radiated noise to the axial separation distance (z) between the propeller and a flat plate representing the wing, as well as the offset separation distance (d) between the propeller and the wing. It was found that the sources arising from propeller–wing interactions are highly directive and are influenced by even and odd number of blades. Additionally, findings indicated a significant increase in both tonal and broadband noise when the wing is placed in an offset position corresponding to the tip vortex flow.

In this paper, we extend the work presented in [6,21] by investigating a more realistic propeller and wing configuration representative of VTOL take off conditions. Whereas ref. [21] reported preliminary measurements with limited analysis, the present study offers an expanded and corrected interpretation of the underlying aeroacoustic mechanisms. The conference version proposed an interpretation of the dominant noise sources that was later found to be incomplete and in some aspects incorrect. In the current work, we revisit these findings using an analytical framework and a detailed examination of the same experimental dataset, which allows us to validate our hypothesis and confirm that unsteady loading is the dominant source mechanism in the take off configuration. In particular, we show how the presence and position of the wing modify the impinging flow, change the balance between propeller and wing contributions, and give rise to additional interaction mechanisms such as unsteady lift and proximity driven modulation effects that were not identified in the earlier study.

In the configuration examined in this study, the propeller plane is parallel to the wing platform and may exhibit partial overlap, a layout commonly found in many fixed-wing VTOL vehicles, particularly those with downstream rotors. The work is primarily experimental and supported by analytical predictions used to identify the key noise generation mechanisms. A parametric investigation is conducted by varying the vertical separation distance z and the horizontal offset or overlap distance d between the propeller and the wing. Far-field acoustic measurements are collected over a wide range of polar and azimuthal angles to assess the sensitivity of noise radiation to these geometric parameters. Flow velocity measurements in the region between the propeller and the wing provide further insight into the dominant noise-generation processes. Overall, the findings offer guidance for the design of low-noise fixed-wing VTOL vehicles and support the development of noise-abatement strategies for urban air mobility and unmanned aircraft operations.

2. Dominant Sources of Noise at Takeoff Configuration at Hover

This study builds upon the research presented by the authors in [6] to explore the dominant noise sources present on a propeller–wing configuration during takeoff. The previous work identified three main categories of noise sources during cruise conditions: (1) propeller self-noise, (2) propeller–wing installation noise, and (3) wing self-noise [6]. However, the possible dominant noise radiation mechanisms during takeoff are more complicated due to the presence of multiple interacting sources, as illustrated in Figure 1, where z and d refer to the axial separation distance between the propeller plane and the wing, and the offset/overlap distance between the propeller axis and the wing leading edge, respectively.

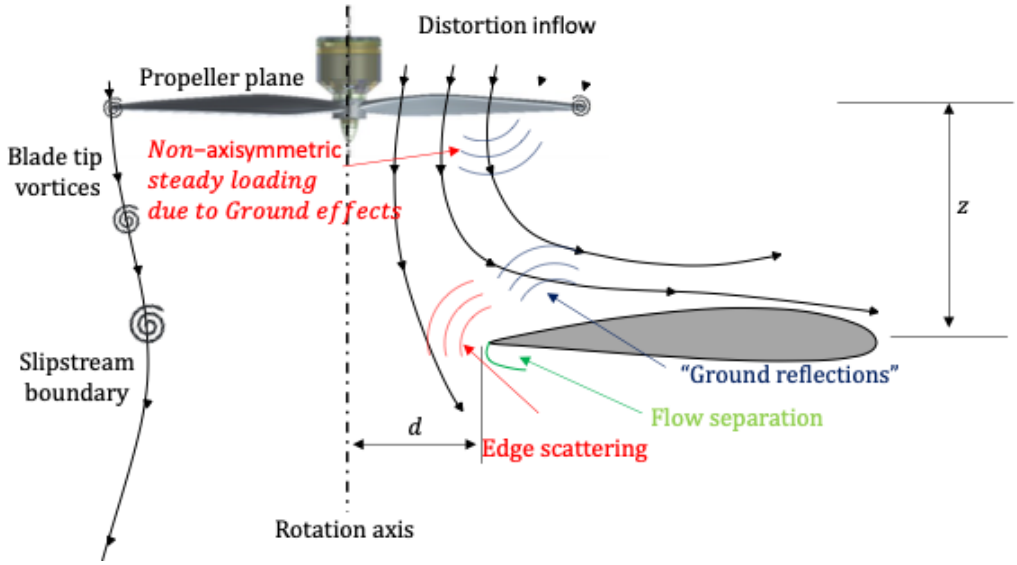

Figure 1. Schematic of the dominant noise sources for a propeller-wing overlapping configuration. The overlap between the propeller disk and the wing induces non-axisymmetric steady loading on the propeller blades and generates distortion inflow. The propeller downwash interacts with the wing's leading edge, causing flow separation and edge scattering. The wing effectively acts as an image source to propeller, generating constructive and destructive interference patterns. The axial separation distance is denoted by z and horizontal offset distance by d. where, D is the diameter of the propeller.

2.1. Radiation from the Propeller

The most significant effect of placing the propeller in close proximity to the wing is that the aerodynamic loading on a single blade varies strongly depending on its blade position relative to the wing. Below are the list of possible sources arising from the propeller:

1. Unsteady propeller loading: The propeller loading fluctuates periodically at the Blade Passing Frequency (BPF) due to the following two effects, leading to the generation of tones at harmonics of BPF.
    (a) Due to partial wing blockage: The most important is due to blockage caused by 'ground effects', which is well documented in the literature [22]. However, the important difference in the case of propeller–wing interaction is that the 'ground effects' only influence the portion of the propeller disc that overlaps with the wing. This results in non-axisymmetric blade loading. This mechanism will be referred to hereafter as 'ground effects', but is always related to the effects of the wing and not of the actual ground below the VTOL vehicle.
    (b) Due to inflow distortion: The second cause of the unsteady blade loading is due to variations in the inflow velocity onto the propeller and the local angle of attack due to the overlap with the wing [23]. This contribution is also shown in the current paper.
2. Acoustic reflections from the wing: Another important effect on the propeller noise due to the wing is that both the tonal and broadband noise spectra become periodically modulated, which we shall show below is due to reflections from the wing when the propeller blades and the wing are overlapped. This behaviour is examined in detail in Section 4.4.1. This mechanism will be referred to hereafter as 'ground reflection effects', which are again related solely to reflections by the wing and not by the ground below the VTOL vehicle.
3. Potential field interactions: Another source of interaction tonal noise is due to the propeller operating in the potential near field of the wing, resulting in a non-axisymmetric

upwash velocity and hence blade loading. Potential interaction noise refers to the tonal noise generated when the propeller interacts with the bound potential field of the wing and vice versa. It is identified by its tonal character and its strong sensitivity to very small separation distances ($z/D < 0.1$, where D is diameter of propeller), consistent with [6,24]. This differs from broadband mechanisms such as turbulent ingestion or loading noise.

2.2. Radiation from the Wing

Noise is also radiated from the wing, which includes both self-noise sources and sources associated with the periodic interaction with the propeller. The dominant sources of propeller–wing interaction at cruise were identified in a recent papers [6,24] and include interactions of the potential near field, viscous wake and tip vortex from the propeller interacting periodically with the wing. However, additional interaction noise sources are generated by the wing at takeoff when flow due to the propeller passes over it. These include:

1. Flow separation: In the overlap region, the flow may separate on the wing due to high incidence, resulting in additional noise at harmonics of the blade passing frequency.
2. Edge scattering: Interactions of the potential near field, viscous wake and tip vortex in these configurations are currently unknown as we could not separate individual noise sources and also we do not have any analytical models for the configuration where flow impinges normal to the wing.
3. Trailing edge interactions: Additional noise generation is observed when the flow passes parallel to the trailing edge of the wing.

In this paper, we will investigate the variation in noise due to changes in separation distances z and d for a scale-model propeller of 16″ diameter propeller in hover, operating close to a NACA2415 airfoil with a chord of 0.259 m and span of 0.9 m. The sources described above are identified in the current work for the first time in the literature for VTOL configurations, and existing analytical models are adapted to explain the experimental results. The balance of sources is likely to be altered for in-flight conditions but this is out of the scope of the current investigation.

3. Experimental Setup and Procedure

3.1. Propeller Rig

The experimental investigation was carried out on a single propeller rig, representative of a mid-size drone, featuring a blade-chord-based Reynolds number of 2×10^5. The rig comprised a rotor driven by a U7-V2.0 KV280 motor from T-Motor, mounted on a MINI45 ATI 6-axis load cell capable of generating a maximum thrust of 50 N for the largest rotor diameter and maximum rotor speeds of 8000 RPM. The electronic speed controller utilised was a Master Mezon 135 opto unit. For the study, commercially available MEJZLIK 16 × 5.5 (3-bladed) propellers with a 16-inch diameter were employed. The choice of an odd-bladed propeller was intentional to amplify propeller–wing interaction noise compared to propeller self-noise, as previously observed in [6]. The exact rotational speed of the propellers was measured using an ICP Laser Tachometer sensor.

Takeoff configurations were considered by using the setup in Figure 2. The propeller–wing separation distance z/D was systematically varied between 0.1 and 0.5, while the wing offset position d/D was adjusted between 0 and 0.75. These adjustments were made using a linear actuator, as depicted in Figure 2. The linear actuator was powered by a NEMA 23 stepper motor, controlled by a Geckodrive 201x stepper motor controller programmed using an Arduino.

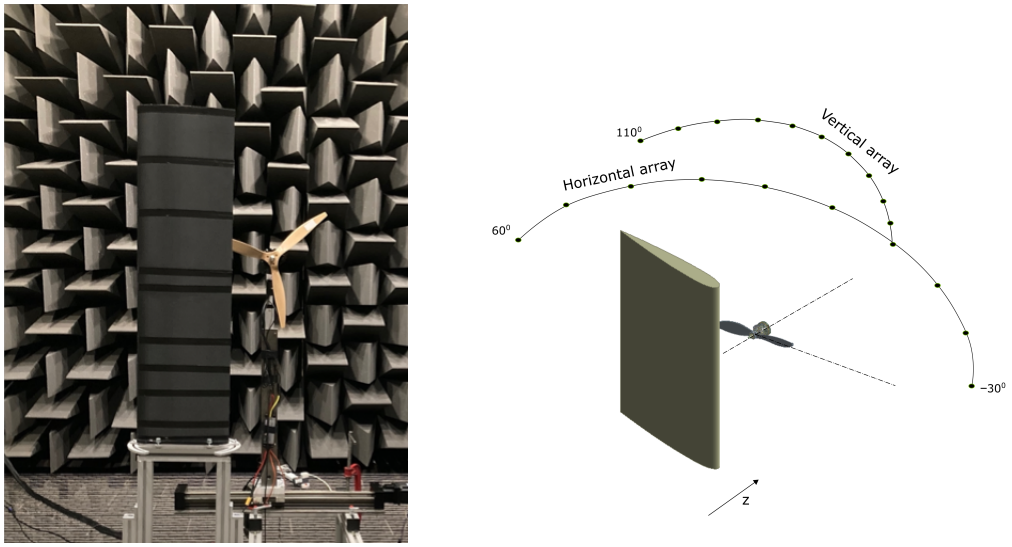

(**a**) (**b**)

Figure 2. (**a**) Photograph of the propeller–wing setup in the ISVR anechoic chamber; (**b**) sketch of the far-field microphone arrays.

3.2. Wing Geometry

This investigation explores two distinct wing geometries: a flat plate aerofoil with a thickness of 5 mm and a realistic wing designed according to the NACA2415 profile. The flat plate aerofoil was honed at both the leading and trailing edges to simulate a zero-thickness flat plate, serving as a means to validate existing analytical theories. Both the flat plate and the aerofoil had a span of 0.9 m and a chord of 0.259 m. The flat plate wing was employed to assess the influence of wing thickness and curvature on the noise signatures.

3.3. Far-Field Noise Measurements

Far-field noise measurements on the propeller–wing rig were conducted within the recently renovated anechoic chamber at the Institute of Sound and Vibration Research, featuring dimensions of 8 m $\times$ 8 m $\times$ 8 m, as illustrated in Figure 2a. The chamber's walls are acoustically treated with foam wedges, characterised by a cut-off frequency estimated to be below 70 Hz.

Far-field noise measurements were obtained by using a vertical and a horizontal microphone array. Both arrays were of a 2 m radius and were centred on the wing leading edge at the mid span. The vertical array incorporated 10 half-inch B&K type 4189 microphones, while the horizontal array featured 11 quarter-inch GRAS 40PL-10 CCP microphones. Figure 2b illustrates the arrangement of the microphones.

The microphones were positioned at emission angles ranging from -30° to 60° relative to the rotor axis and 0° to 100° in the vertical/azimuthal axis. Measurements were conducted over a 20-s duration at a sampling frequency of 50 kHz. The noise spectra were calculated, corresponding to a frequency resolution of 24.42 Hz and a Bandwidth-Time (BT) product of approximately 500. This value ensures a negligible variance in the spectral estimates at the specified frequency resolution. Based on standard practice for such measurements, the uncertainty in the far-field pressure levels is typically within 0.5 dB. We also verified that all measurements were repeatable under the same operating conditions. Therefore, differences smaller than this value should be interpreted with caution.

Sound Power Level spectra $PWL(\omega) = 10\log_{10}(S_W(\omega)/W_{ref})$ were calculated by integrating the Power Spectral Density (PSD) of the far-field acoustic intensity,

$$S_W(\omega) = \sum_{i=1}^{N-1} \frac{[S_{PP}(\omega, \theta_i) + S_{PP}(\omega, \theta_{i+1})]\pi R^2 \cos(\theta)\Delta\theta_i}{\rho c} \quad (1)$$

where $S_W(\omega)$ is the sound power spectral density, $W_{\text{ref}} = 10^{-12}$ W, $S_{pp}(\omega, \theta_i)$ is the PSD measured at a measurement angle θ_i, N is the number of microphones, R is the radius of the microphone array (2 m), $\Delta\theta$ is the angle between the two adjacent microphones, ρ is the density of the ambient air, and c is the speed of sound. Note that the horizontal microphone array is employed to assess the sound power spectrum and overall sound power levels, as our current study is focused on characterising propeller–wing interaction noise. Nonetheless, analogous trends emerge when utilising vertical array data to compute sound power levels. Both arrays are employed to pinpoint the dominant noise source based on its directional characteristics.

To prevent recirculation effects, the rotor was positioned approximately 1.5 m above the ground. A time-frequency analysis was conducted to explore the impact of recirculation on radiated noise, revealing negligible differences. The noise measurements were found to be insensitive to rig positioning in the anechoic chamber, suggesting that recirculation does not significantly affect radiated noise.

3.4. Hot-Wire Measurements

Hot-wire anemometer measurements were also conducted to analyse the steady and unsteady flow field between the propeller and the wing, providing insights into the characteristics of the impinging flow. The HWA used is a Dantec Constant Temperature Anemometry (CTA) equipped with a cross-wire hot-wire probe (55 P61) which was calibrated in a Dantec Dynamics jet stream calibrator for velocities from 0.5 m/s up to 40 m/s and flow angles between -40° to 40°. The hot-wire probe was mounted on a three-axis ISEL traverse system, which precisely locates the hot-wire to the desired measurement position with an accuracy of 0.1 mm. The measurements at each point were conducted for a duration of 10 s with a sampling frequency of 40,000 Hz. The hot-wire probe was traversed along 44 predefined radial locations from hub to tip of the propeller blade for axial locations situated 3 cm upstream of the propeller and 3 cm above the wing. The measurements were conducted for four separation distances (z/D) at a constant thrust of 10 N, where D is the diameter of the propeller. A cross-wire probe was used and the measurements were repeated with the probe oriented horizontally and vertically to capture the three velocity components. "It is important to note that the acoustic and hot-wire measurements were performed independently, but using the same experimental setup. This approach was adopted to eliminate any influence of the hot-wire installation on the acoustic measurements."

3.5. Configurations Tested

Acoustic far-field pressure measurements were performed at a fixed thrust of 10 N for a range of vertical separation distances z/D from 0.1 to 0.5 and wing offset or overlap positions d/D from 0 to 0.75, using a three-bladed propeller in a takeoff configuration. Here, D is the propeller diameter (16 inches). For comparison, the noise generated by a single rotor in isolation was also measured at the same fixed thrust of 10 N. In the literature, there is no universal agreement on whether RPM or thrust should be held constant, as both approaches involve trade-offs. If RPM is held constant, the resulting change in thrust alters the steady loading on the propeller, which influences the loading noise and complicates interpretation. For this reason, we chose to maintain constant thrust, as this is consistent with practical operation where the vehicle must support a known weight.

4. Acoustic Results

4.1. Source Balance

This section presents the results of the parametric study on the overall noise variation with overlap distance d/D and separation distance z/D for the takeoff configuration on a flat plate. Figure 3 shows the variation in overall sound pressure level with overlap distance d for fixed separation distances z/D of 0.1, 0.25, and 0.5 at a fixed thrust of 10 N. The horizontal microphone array is used to calculate the sound power, and the frequency range of 100 Hz to 10,000 Hz is considered to calculate the overall sound power levels. For the isolated rotor case, the overall sound power levels are also plotted for comparison across the different separation distances, even though no wing is present. This is done to remove any uncertainty in interpreting the trends. As expected, the variation in the OAPWL for the rotor alone remains essentially constant because there is no wing to influence the noise radiation. Figure 4 shows a similar variation for broadband noise level. The following key observations can be made from these figures:

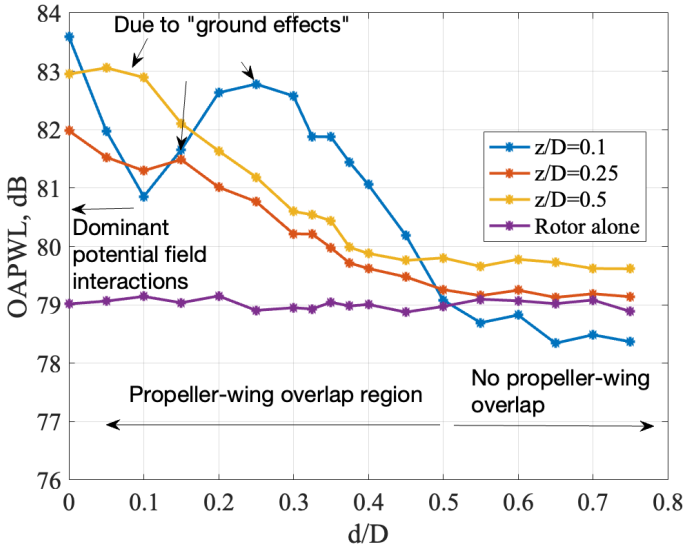

Figure 3. Overall sound power level (tonal + broadband) variation with overlap distance d/D for three different z/D at 10 N thrust.

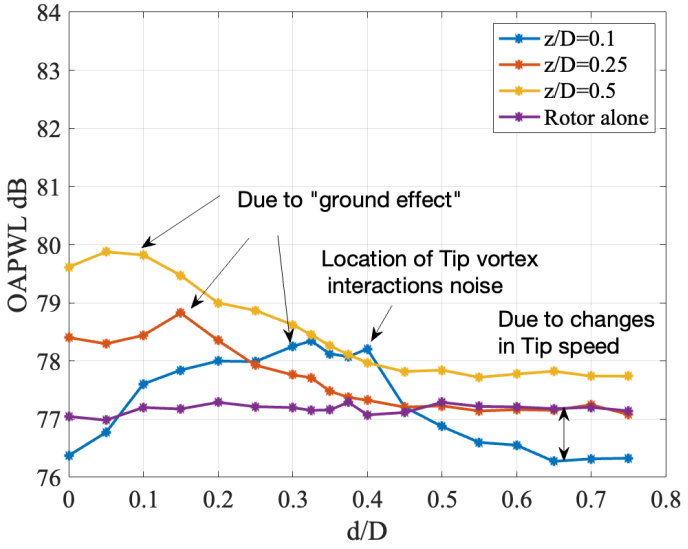

Figure 4. Broadband sound power level variation with overlap distance d/D for three different z/D at 10 N thrust.

- For overlap distances ($d/D < 0.5$), the interaction noise sources make a significant contribution to the overall noise compared to the rotor self-noise. As d/D increases beyond 0.5, the overall noise tends to collapse with the rotor self-noise, indicating the accuracy of the measurements. However, for $z/D = 0.1$ and $d/D > 0.5$, the rotor alone slightly dominates the total interaction noise by 0.5 dB. This is due to the slight decrease in the RPM of the propeller for small z/D to maintain the same thrust which was set for lower d/D, which effectively leads to lower self-noise.
- At a lower separation distance of $z/D = 0.1$, two distinct peaks appear in the overall sound power level when plotted against overlapping distance d/D. The first peak is possibly linked to the impact of potential field interaction for smaller overlaps ($d/D < 0.1$), while the second peak ($d/D \approx 0.25$) is associated with asymmetric lift on the propeller due to wing overlap. An additional interaction source emerges due to tip vortex flow around $d/D \approx 0.35$. Notably, the location of maximum tip vortex interactions ($d/D \approx 0.375$) aligns precisely with the tip vortex's location measured by the hot wire, which will be detailed in subsequent sections. Furthermore, a peak around $d/D = 0.35$ in broadband noise level is observed, representing peak rms fluctuations in the tip vortex flow at $z/D = 0.1$. The subsequent Section 4.2 provides a detailed exploration of these observations and the underlying reasons behind them.
- With the increase in z/D, interactions occur at smaller overlap regions due to slipstream contraction. Similar patterns are evident in both total and broadband noise levels for z/D values of 0.25 and 0.5. The rise in broadband noise is likely attributed to 'ground reflection effects' associated with acoustic reflection from the wing. This mechanism and its role in the larger broadband noise when increasing z/D is discussed in Section 4.4, where a simplified model is also presented to support our hypothesis.

A more thorough interpretation of the above observations will be provided in Section 4.4.

To investigate the spectral behaviour, we now present the sensitivity of the sound power level spectra to separation and overlap distances z and d. In Figure 5a, sound power level spectra are plotted against blade passing frequency for two different overlap distances (d/D of 0 and 0.25) at a fixed separation distance (z/D of 0.1) for the takeoff configuration. The sound power level spectra for the isolated rotor are also plotted for comparison. The installed noise spectra is clearly higher across all frequencies compared to the rotor alone case.

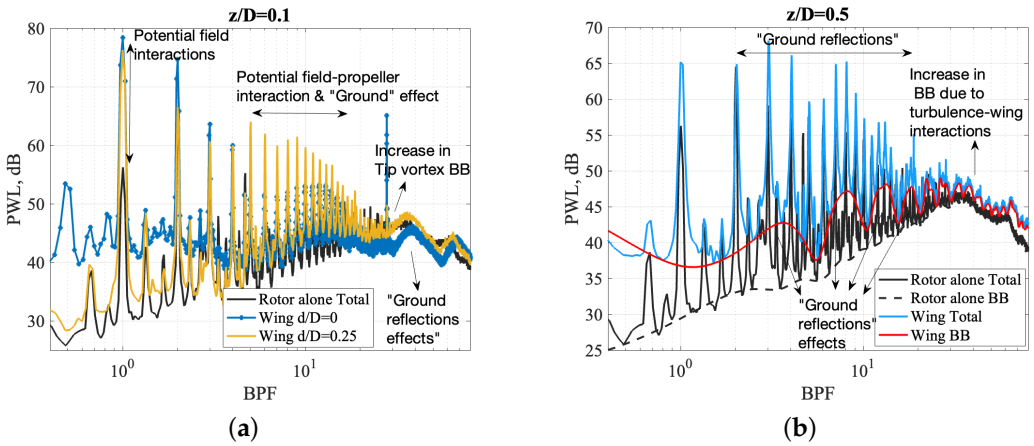

(**a**) (**b**)

Figure 5. Sound power spectra comparison for rotor-alone and propeller–wing configurations at 10 N thrust: (**a**) $z/D = 0.1$, $d/D = 0$ and $d/D = 0.25$; (**b**) $z/D = 0.5$, $d/D = 0$.

In both installed wing configurations ($d/D = 0$ and 0.25) shown in Figure 5a, a clear increase in the 1BPF (1st Blade Passage Frequency) tone is observed. This increase is likely

to be attributed to potential field interactions and unsteady propeller loading due to the wing for the cases of $d/D = 0$ and $d/D = 0.25$ respectively. Additional sources of noise also arise from the distorted inflow onto the propeller. An estimate for the effect on noise caused by unsteady propeller loading due to 'ground' effects and inflow distortion are given in Section 4.4 below. We demonstrate in Section 4.4.2 that the increase in higher harmonic amplitudes at $d/D = 0.25$ can be explained by the unsteady propeller loading due to the 'Ground effect'. In addition to rotor noise, there is also a noise contribution from the wing due to flow from the rotor impinging close to perpendicularly to the wing platform, for which no models are currently available. It is therefore not possible to estimate the noise radiated by the wing.

At very small separation distances, another source of tonal noise arises from scattering of the propeller potential field by the wing. However, a detailed numerical study of the noise due to propeller–wing configuration is required to quantify these sources accurately.

In addition to the effect on the tonal amplitudes discussed above a distinct increase in broadband noise can be observed at frequencies higher than about the 20th blade passing frequency. In the presence of the wing, the broadband noise spectrum is oscillatory. This oscillatory behaviour is indicative of interference between the direct field from the propeller and the reflected field from the wing, leading to constructive and destructive interference at frequencies corresponding to the peaks and dips observed in the broadband spectra. This interference phenomenon will discussed in detail in Section 4.4.

The sound power level spectra are plotted in Figure 5b as a function of blade passing frequency for a fixed separation distance (z/D of 0.5) and a fixed overlap distance (d/D of 0). Also included is the rotor-alone noise and the corresponding broadband noise spectrum. Figure 5b shows clearly that, in the presence of the wing, a distinct increase in both tonal and broadband noise is observed.

The increase in broadband noise is believed to arise due to the interaction between the unsteady flow predominantly due to the tip vortex and the wing leading edge. Flow measurements in between the propeller and the wing provide insights into the presence of turbulent tip vortex structures for the cases $r/R < 0.5$, attributable to vortex pairing taking place at greater downstream distances.

One of the prominent features observed in the spectra of Figure 5b is a modulation of the broadband and tonal spectrum occurring at lower frequencies. As the vertical separation distance z between propeller and wing is increased, the influence of the wing ("ground effect") becomes evident at the lower blade passing frequencies, in the form of a modulation of the frequency spectrum. Further interpretation of the reasons behind these modulations is provided in Section 4.4.

To illustrate the effect of the wing on individual blade passing frequencies, Figure 6a,b shows the overall sound power level at 1BPF, the overall sound power level, and the overall total and broadband levels individually in the frequency band between the 7th and 9th BPF for two different separation distances of z/D of 0.1 and 0.5. This frequency range is selected to assess the dominant noise source harmonics that govern the behaviour of the variation for OAPWL with d/D shown in Figure 3. At the smaller separation distance of $z/D = 0.1$, the 1st Blade Passage Frequency is the dominant tone, which can be attributed to contributions from the potential fields scattered by the propeller and wing and the unsteady loading noise from the propeller due to reflections from the wing. In Section 4.4, qualitative explanations are provided to shed light on these contributions. By contrast, at the larger separation distance of $z/D = 0.5$, the dominant total and broadband contributions occur in the frequency range between the 7th and 9th Blade Passage Frequencies, which explains the overall OAPWL trends observed in Figure 3. These contributions are primarily attributed to reflections from the wing, which could potentially amplify the tonal and broadband

components at these blade passing frequencies. A simple model is presented in Section 4.4 to explain this phenomenon.

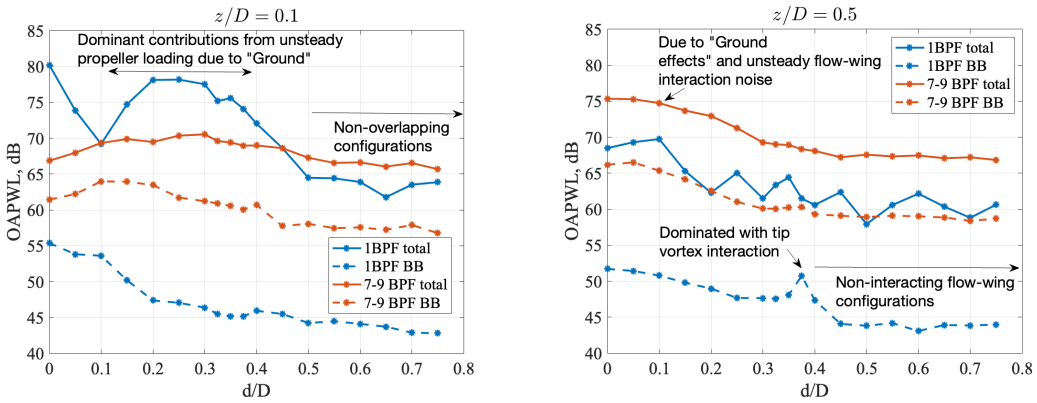

(**a**) (**b**)

Figure 6. Variation in sound power level for 1BPF and 7–9 BPF plotted against d/D at fixed separation distances: (**a**) $z/D = 0.1$; (**b**) $z/D = 0.5$.

4.2. Comparison Between Aerofoil and Wing

We now present the results of a parametric study into the noise variation with overlap separation distance d/D at various z/D values ranging from 0.1 to 0.5 for a NACA2415 wing. We first assess the effect of wing geometry on interaction noise by comparing the noise radiation from a flat plate with that from a realistic aerofoil adjacent to the propeller.

Figure 7a shows a comparison between the overall radiated sound power level for aerofoils and flat plates, plotted against d/D for $z/D = 0.1$. It is evident that the overall trends for both configurations are nearly identical, with differences of up to 1 dB observed for $d/D > 0.5$.

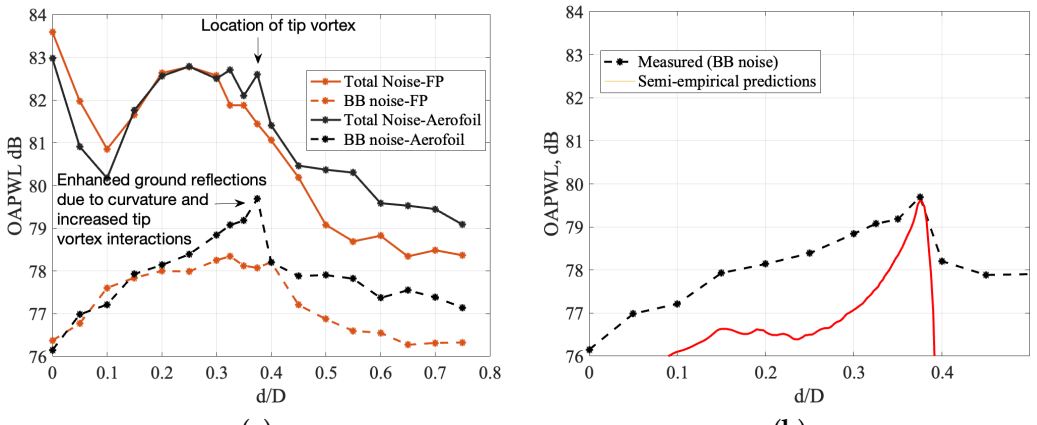

(**a**) (**b**)

Figure 7. (**a**) Overall sound power level vs. d/D for flat plate and aerofoil at $z/D = 0.1$ and 10 N thrust; (**b**) measured vs. predicted broadband interaction noise.

These differences primarily arise from the flow behaviour between the propeller and flat plates (at $d/D < 0.15$) and the tip vortex interactions for the wing (at $d/D \approx 0.375$). The curvature of the aerofoil may provide a possible explanation for these discrepancies. However, as the separation distance increases (at $d/D > 0.375$), the differences between the flat plate and aerofoil configurations become more pronounced due to changes in the RPM. In particular, noise from the aerofoil configuration is higher as the propeller is operating at slightly higher RPM compared to the flat plate case due to higher blockage.

Figure 7b shows the variation in broadband sound power level plotted against d/D for $z/D = 0.1$. An approximate prediction of the noise from unsteady flow-wing interactions

is included based on the simple assumption that the unsteady force generated by the jet striking the wing is proportional to $\frac{1}{2}\rho A U^2$, where U is the velocity of the unsteady flow onto the wing. Currently, there is no aerofoil response model for the case when a gust convects onto an aerofoil perpendicular to the chord in which a shear layer is generated. Thus, in the prediction we make the assumption that the far-field pressure is proportional to $U^3 u_{rms}^2$ [25], based on the measured flow field U and u_{rms} in the absence of the wing (later shown in Section 4.3.2), as our objective is to capture the tip vortex interactions. The plotted results exhibit a good agreement with the precise location of the tip vortex structure, thereby demonstrating that the increase in broadband noise is indeed due to intensified tip vortex-wing interaction noise.

We now investigate the effect on the rotor noise spectrum due to varying the overlap distance d/D at the constant thrust of 10 N. The total radiated sound power spectrum is plotted in Figure 8a,b against frequency normalised by the blade passing frequency for the flat plate and aerofoil configurations respectively, at a separation distance of z/D of 0.2. The blade passing frequency tones and their modulations are clearly visible and similar between the flat plate wing and the aerofoil wing. It is clear from the Figure that the presence of 'ground effects' is amplified in the frequency range of 6–15 BPF for the case of aerofoil. This enhancement could be attributed to the curvature of the aerofoil and the axisymmetric unsteady lift on the propeller, which intensifies the interaction source in addition to tip vortex interactions. However, the specific contribution of ground effects remains uncertain and requires further investigation.

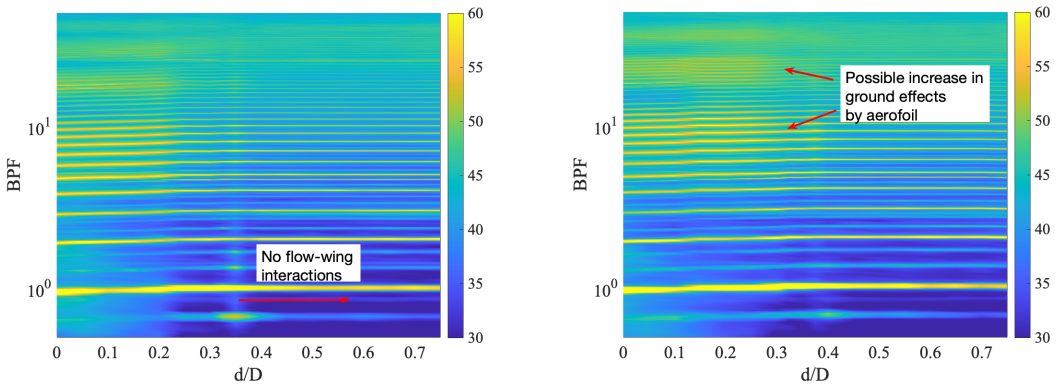

(**a**) Flat plate (**b**) Aerofoil

Figure 8. Sound power level (in dB) contours vs. non-dimensional distance d/D and BPF at 10 N at $z/D = 0.2$: (**a**) flat plate; (**b**) aerofoil.

4.3. Flow Measurements

To analyse the flow characteristics around the propeller–wing configuration, comprehensive velocity measurements were conducted using hot-wire anemometry. The measurements were carried out at a fixed thrust of 10 N, and the following measurements were performed, as illustrated in the schematic diagram shown in Figure 9:

1. Propeller-Alone Downstream Flow: We measured the velocity at various positions downstream of the propeller (at z/D values of 0.1, 0.25, and 0.5) across all radial locations.
2. Propeller-Alone Upstream Inflow: The velocity was measured at a location situated 3 cm above the propeller plane, capturing the upstream inflow across all radial positions.
3. Propeller Plus Wing at d/D = 0.25 and z/D = 0.1: In this configuration, we measured the downstream flow and upstream inflow velocities across all radial locations.

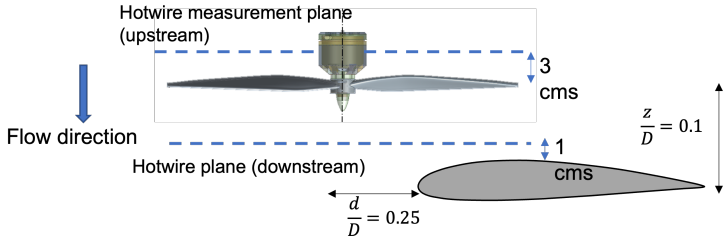

Figure 9. Schematic of the hot-wire measurement planes. Measurements are also taken without the wing.

These measurements aim to derive a detailed understanding of the flow behaviour in the vicinity of the propeller–wing configuration and provide valuable insight into the velocity distribution, allowing us to assess the dominant interaction noise sources.

4.3.1. Inflow Characteristics

The goal of this section is to characterise the inflow distortion impinging on the rotor so that the mean flow velocities can be used in the analytical model to predict the noise generated due to inflow distortion. Figure 10a,b shows the mean axial velocity contours for the rotor alone and with-wing configuration at $d/D = 0.25$ and $z/D = 0.1$. The position of the plate is shown by the red dotted line on the Figure. Figure 10b clearly shows a distorted inflow into the propeller due to re-circulation caused by the downstream wing as shown in the schematic in Figure 1. Figure 10c,d shows the rms velocity contours of the axial velocity flow. Naturally, the flow into the propeller can be observed to be non-axisymmetric and contain high levels of turbulence, particularly in the shear layers.

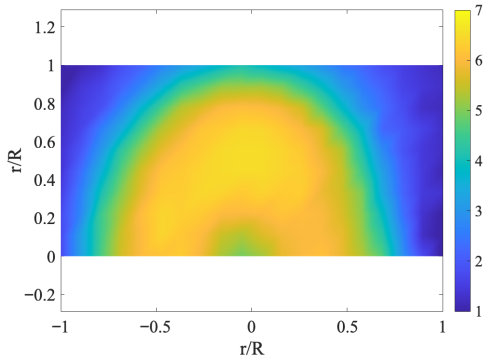

(**a**) Propeller alone: axial mean velocity.

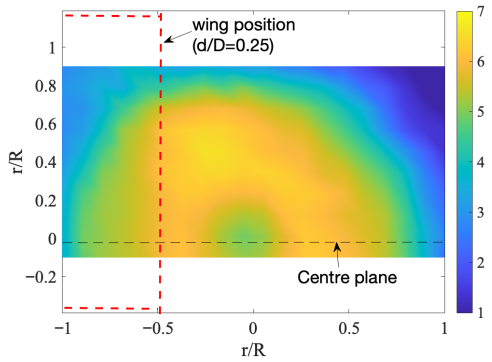

(**b**) Propeller next to wing: axial mean velocity.

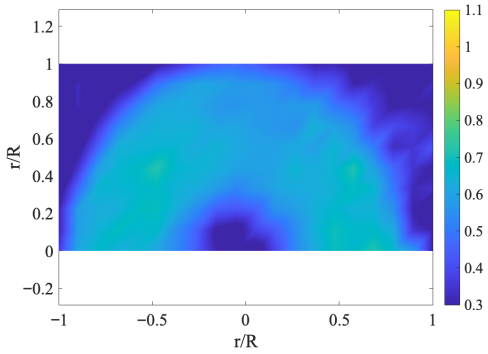

(**c**) Propeller alone: axial RMS velocity.

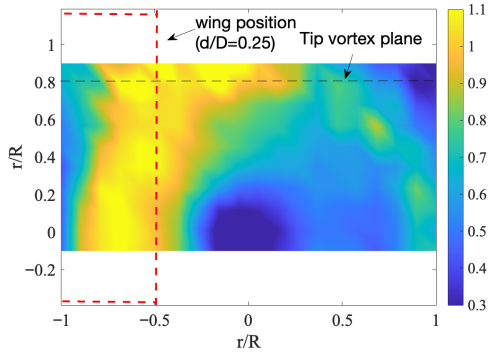

(**d**) Propeller next to wing: axial RMS velocity.

Figure 10. Axial mean (**a**,**b**) and RMS velocity (**c**,**d**) contours upstream of the propeller (in m/s) for: (**a**,**c**) propeller alone and (**b**,**d**) propeller next to a wing located at $d/D = 0.25$ and $z/D = 0.1$.

Hot-wire velocity spectra were measured at the centre and tip planes (dashed line shown in Figure 10b,d) are plotted against blade passing frequency in Figure 11a,b. Tonal

amplitudes at the blade passing frequencies are observed to be more pronounced at the position where recirculation occurs due to wing overlap. An increase in broadband velocity spectra close to the tip is also observed which is likely to contribute to broadband interaction noise, as previously observed in Figure 7.

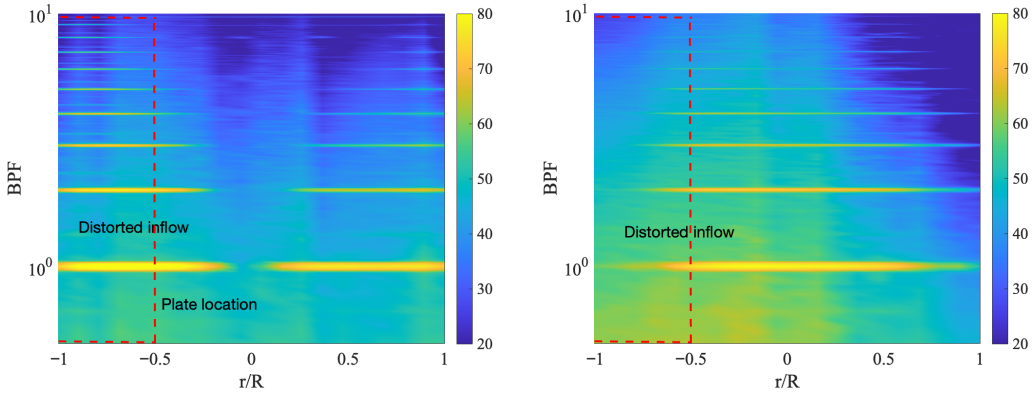

(**a**) Centre plane. (**b**) Tip vortex plane.

Figure 11. PSD of the distortion flow (in dB) taken at the location of (**a**) centre plane and (**b**) tip vortex plane.

4.3.2. Wake and Tip Vortex Characteristics

This section describes the results of the velocity measurements conducted at the blade tip where the tip vortex dominates, and at downstream positions where the propeller wake dominates. Velocity measurements were made at the blade tip to attempt to track the evolution of the tip vortex with and without the presence of the wing placed around d/D of 0.25 and z/D of 0.1. Two orientations of cross-wire probes were used to measure all three components of velocity.

Figure 12a–c presents the ensemble-averaged axial mean velocity contours for different downstream values of z/D of 0.1, 0.25 and 0.5, respectively. As discussed previously, the location of the tip vortex is around $r/R = 0.75$ for $z/D = 0.1$ and then moves inward towards the hub as z/D is increased. It is also observed that the tip vortex grows in size with increasing z/D and breaks down around z/D=0.25, especially in hover condition.

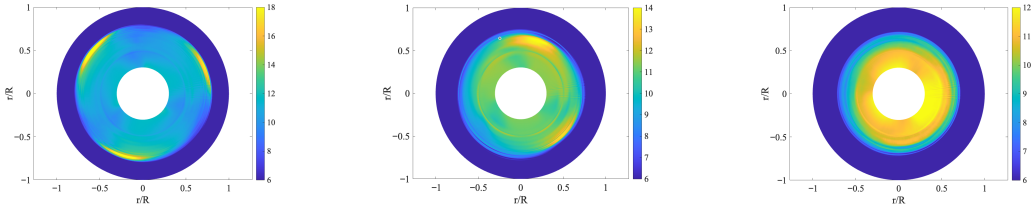

(**a**) $z/D = 0.1$. (**b**) $z/D = 0.25$. (**c**) $z/D = 0.5$.

Figure 12. Axial mean velocity contours (in m/s) ensemble-averaged over multiple revolutions: (**a**) $z/D = 0.1$; (**b**) $z/D = 0.25$; (**c**) $z/D = 0.5$.

The flow behaviour between the propeller plane and a flat plate wing is characterised using hot-wire probes in order to quantify the propeller wake characteristics due to the 'ground effects' of the wing. Figure 13a shows the axial velocity contours on the wing at $r/R = 0.5$ ($d/D = 0.25$). The overlap region is represented by $r/R < -0.5$. In the diagram, the velocity on the right side corresponds to the conventional wake and tip flow, while the velocity on the wing below $r/R < -0.5$ indicates the development of a wall jet on the wing surface. Similarly, Figure 13b shows the corresponding root mean square (rms) velocity contours. Significantly higher levels of rms fluctuations are observed within the flow recirculation region, which has the potential to contribute to both tonal and broadband propeller interaction noise.

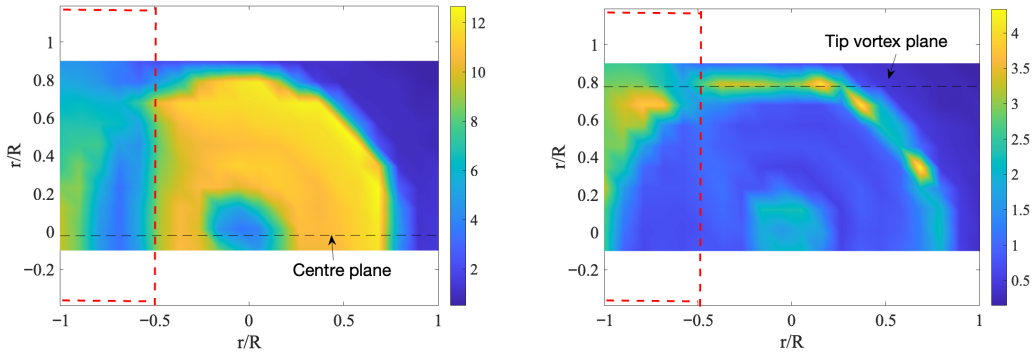

Figure 13. Axial (**a**) mean and (**b**) RMS velocity contours (in m/s) in the region between the propeller and wing for $d/D = 0.25$ and $z/D = 0.1$. The red dashed box representing the wing position.

One key observation from these velocity contours is that for smaller separation distances ($z/D \approx 0.1$), the flow around the wing undergoes significant changes compared to the case without the wing. This alteration in the flow results in enhanced lift on the propeller blades during overlap, primarily due to the bluff-body effects caused by the presence of the wing. Such changes in the flow field can substantially influence the aerodynamic and acoustic characteristics of the propeller–wing interaction. These 'ground effects' on propellers have been previously noted by [22].

Hot-wire velocity spectra were measured at two plane locations: centre and tip vortex plane (dashed line shown in Figure 13a,b). These are plotted against blade passing frequency in Figure 14. It is clear that a strong flow re-circulation region is observed in the tip vortex plane which is forced at the blade passing frequency. However, more analysis and a new analytical framework are required to precisely understand the relationship between the velocity measurements with the radiated noise as the relative source balance changes for various overlapping distances d/D. High-fidelity computational fluid dynamics (CFD) simulations could also provide additional insight into the hypothesised noise generation mechanisms proposed here.

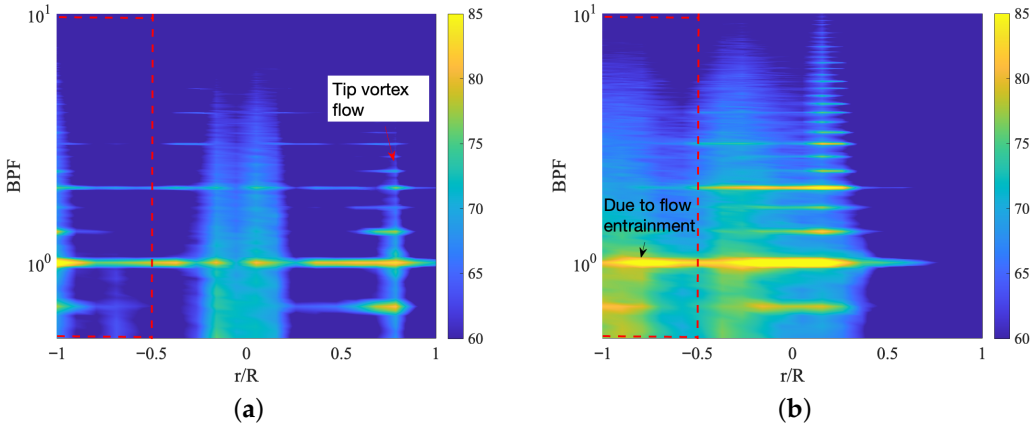

Figure 14. PSD of the velocity fluctuations (in dB) measured in the region between the propeller and wing at $d/D = 0.25$ and $z/D = 0.1$, for the planes shown in Figure 13: (**a**) centre plane; (**b**) tip vortex plane. The red dashed box representing the wing position.

4.4. Interpretation: Radiation from Propeller

4.4.1. Role of Acoustic Reflections from the Wing

In this section, we investigate in detail the effects on the noise spectrum due to variations in the vertical separation distance z between the propeller and wing. From here on we shall refer to this phenomenon as the 'ground effect' due to its strong similarity

with the effects of the ground caused by recirculation and reflections. The broadband noise spectra for different separation distances (z/D) are plotted in Figure 15 against Strouhal number $St = fz/c_0$, where c_0 is the speed of sound. The spectra are found to collapse with distinct peaks and dips at frequencies fz/c_0 = [0.3, 0.9, 1.4, ...] and fz/c_0 = [0.6, 1.1, 1.6, ...], respectively, suggesting strong interference effects between the propeller noise incident upon the wing and its reflection.

The interference spectra observed in Figure 15 are also compared against the simple expression for sound power W due to a vertical point dipole source above a rigid plane boundary [26],

$$\frac{W}{W_f} = 1 - \frac{3}{2kz}\left[\left(1 - \frac{2}{(2kz)^2}\right)\sin 2kz + \frac{2}{2kz}\cos 2kz\right], \quad (2)$$

where W_f is the power radiated in free-field and k is the acoustic wavenumber ω/c. A vertical dipole point source is suggested in this case as a representative approximation of the different broadband propeller noise sources over the plate/wing.

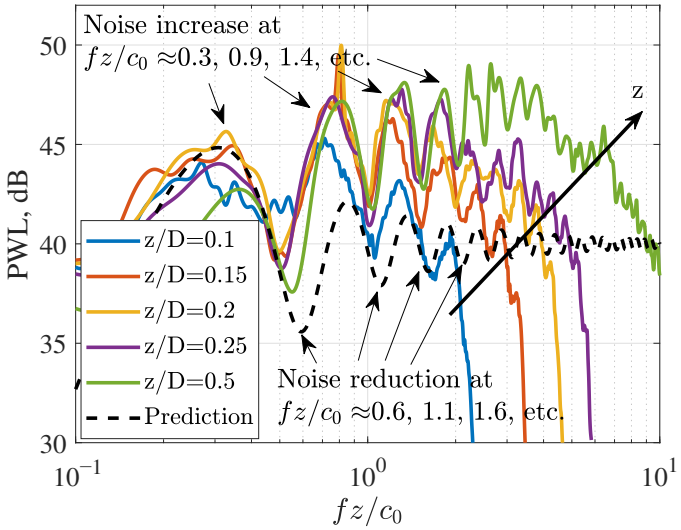

Figure 15. Broadband noise spectra for different separation distances (z/D) and predicted ground reflection effects.

The peaks and dips in the broadband noise spectra are found to closely follow those obtained from the simple prediction model. Agreement between the theory and measurement highlight two important issues related to propeller—wing interaction. The first is that the wing behaves similar to an infinite rigid plane, the second is that the effective source distribution behaves as a point source, suggesting that the source mechanism is highly localised, such as from a tip vortex for example. This reflection phenomenon becomes particularly pronounced for large $z/D > 0.2$, for example in vertical takeoff configurations, where the propellers overlap the wing. The amplification of low frequencies due to the 'Ground effect' leads to enhanced overall sound power radiation, as depicted in Figure 3.

4.4.2. Role of Unsteady Lift Due to 'Ground' Effect

The presence of a wing in close proximity to a propeller causes azimuthal variations in the mean flow onto the propeller, which in turn creates an azimuthal variation in blade loading as the blades move towards the wing and away from it. As we shall demonstrate below, an azimuthal variation in blade loading generates acoustic modes that are able to propagate efficiently to the far field. By contrast, when the blade loading is uniform around the propeller disc, acoustic modes are 'locked' to the propeller. At subsonic tip speeds, these spinning modes rotate with a phase speed that is slower than the speed

of sound and therefore radiates efficiently. We now present the underlying theoretical framework for describing this noise generation mechanism, based on the formulation due to Goldstein [27]. We emphasise that the goal of this model is not to develop a precise prediction tool, but rather to validate our hypothesis and to show that the unsteady loading due to ground effect can be a potential source of noise.

In the presence of a wing, or any other body, the variation in thrust per projected area acting on a particular blade assumed to be in the plane $x' = 0$ with radial and azimuthal position (r', ϕ') and source time τ is $f_T^0(r', \phi', \tau)$ around the propeller disc. As the propeller passes over the wing it experiences an increase in lift due to a reduction in the downward flow of air through the rotor, which results in a pressure change in the wake that decreases the inflow to the rotor. Due to the periodicity of f_T^0 with ϕ' the thrust variation must also be periodic in τ, which may therefore be represented as a sum of single frequency components at harmonics of the blade passing frequency, whose pth Fourier coefficient is given by

$$F_{T,p}^0(r', \phi') = \frac{\Omega}{2\pi} \int_0^{2\pi/B} e^{ip\Omega\tau} f_T^0(r', \phi', \tau) d\tau, \tag{3}$$

Following Goldstein [27] the amplitude of the n-th harmonic of the acoustic pressure at a far-field observer position $\mathbf{x}$ with spherical coordinates x, θ, and ϕ, is given by,

$$\begin{aligned} p_{nB}(\mathbf{x}) = \frac{iBk_{nB}}{4\pi x} e^{ik_{nB}x} \sum_{p=-\infty}^{\infty} e^{i(nB-p)(\phi-\pi/2)} \int_{A_0} J_{nB-p}(k_{nB} r' \sin\theta) \cdot \\ e^{ip\phi' - inB\phi'} \left(\cos\theta F_{T,p}^0(r', \phi') - \frac{nB-p}{k_{nB} r'} F_{D,p}^0(r', \phi') \right) r' dr' d\phi', \end{aligned} \tag{4}$$

where B is the number of blades, c_0 is the speed of sound, $k_{nB} = nB\Omega/c_0$ is the acoustic wavenumber at the nth harmonic of the rotational frequency Ω, A_0 is the propeller blade surface.

The geometry of the propeller and wing configuration is sketched in Figure 16 below. In the figure, a propeller of diameter D is rotating in close proximity to a wing whose centre of rotation is at a distance d from the wing leading edge.

By simple geometry, the propeller tip begins to overlap the wing at the azimuthal angle α when $(D/2)\cos(\phi_c') = d$. The angle of overlap α is therefore given by

$$\phi_c' = \cos^{-1} \frac{2d}{D} \tag{5}$$

One of the main objectives of this paper is to demonstrate that, at the critical separation distance of $d/D \approx 0.25$, maximum noise is produced by the propeller. This effect is most pronounced at small propeller–wing vertical separation distances of $z/D < 0.25$, where the unsteady loading noise from the propeller is dominant. To illustrate the effect of unsteady blade loading due to wing overlap, we investigate the solution to Equation (4) for an idealised case in which the propeller is assumed to behave as a rotating point force located at the propeller tip whose strength follows a Gaussian variation as it passes over the wing. We assume that the force variation with blade angle ϕ' over a single rotation is of the form,

$$f_T(\phi') = f_T^0 + f_0 \frac{1}{2\pi\sqrt{3\phi_c'}} e^{-(\phi'/3\phi_c')^2} \tag{6}$$

where f_T^0 is the steady thrust on the blade at positions well away from the wing, f_0 is the maximum increase in thrust at maximum overlap and ϕ' is the blade angle measured from the horizontal and ϕ_c' is the angle at which the propeller tip just overlaps with the wing. The constant of 3 introduced in Equation (6) is chosen arbitrarily so that the additional thrust is e^{-3}, (5%) of the maximum additional thrust at full overlap $\phi' = 0$. This force

variation is defined to maintain constant integrated lift independent of overlap d, i.e., $\int_0^\infty f_T(\tau)d\tau = 1$. The force variation versus source time τ may be deduced from $f_T(\phi')$ by noting that $\phi' = \Omega\tau$, defined such that the blade is in the full overlap position at $\tau = 0$ and assuming that the force is periodic at the blade passing frequency. However, in reality, with a decrease in wing overlap, σ also decreases. Additionally, f_0 is also a function of the spanwise position. Precise variations cannot be determined without numerical simulations, which is beyond the scope of the current paper.

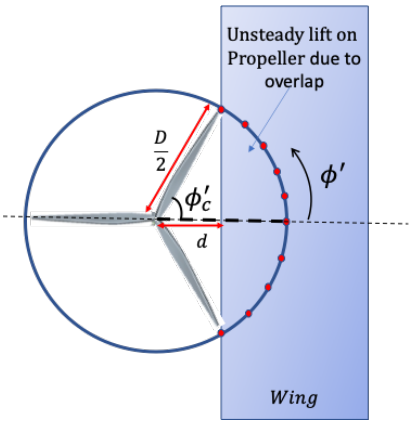

Figure 16. Schematic of the propeller–wing overlapping system demonstrating the overlapping angle ϕ'_c.

Using the simple model of Equation (4) we now investigate the effect on noise radiation due to varying overlap distance d. In these simulations, we assume that the maximum increase in unsteady lift f_0 due to overlap with the wing remains constant at all overlap distances d and equal to $f_0/f_T^0 = 0.15$ following the measurements of [22].

The force variations obtained from Equation (6) were input to Equations (4) and (5) to compute the radiated sound pressure level for all overlapping distances d. The sound power levels were then determined by integrating the far-field intensity over the same range of angles used to make the noise measurements. Figure 17 shows contours of the predicted sound power levels plotted against harmonics of the BPF and overlap distance d/D.

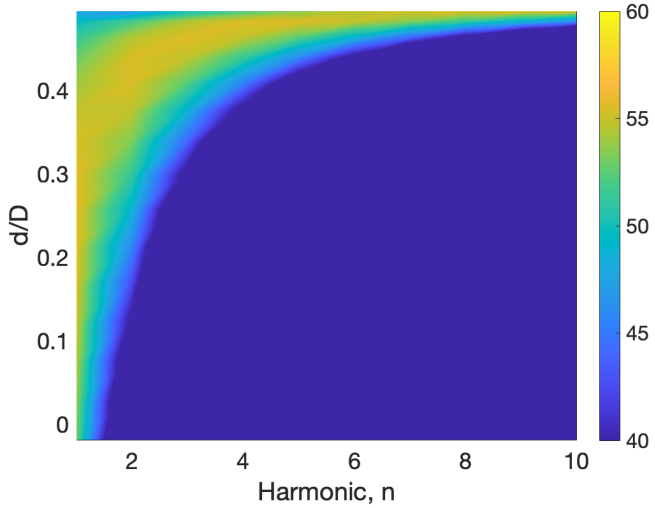

Figure 17. Sound power level contours (in dB) plotted against blade passing harmonics, n and overlapping distance, d/D.

The predicted noise spectra can be observed to increase in level and become broader as the degree of overlap reduces, while maintaining constant integrated additional thrust for

all overlap distances. The values corresponding to $d/D = 0$ are similar to the spectrum of the baseline case without wing, where the propeller thrust remains constant at all time τ. In this case, the sound power is predicted to decrease exponentially with frequency harmonic n. This phenomenon arises because the acoustic modes are locked to the propeller and therefore rotate subsonically, the efficiency of radiation becoming progressively weaker with increasing harmonic order n.

However, at the lowest level of overlap, the noise radiation is greatest (assuming constant integrated thrust). At this condition of least overlap the thrust amplitude spectrum $F^0_{T,p}$ is 'flattest' implying that thrust harmonics of large p order contribute more to the relative noise radiation than when the propeller–wing overlap is greater. Thrust components of large p scatter into low-order acoustic modes of order $m = nB - p$, which radiate more efficiently across all frequency harmonics n. It is clear, therefore, that the presence of the wing causes a significant increase in tonal amplitudes, particularly at the higher harmonic frequencies n.

Figure 18 compares the variation in sound power level at the first blade-passing frequency (BPF) plotted against the overlap distance d/D for both predicted and measured data. The predicted values are adjusted by 20 dB for this comparison to allow direct comparison. Figure 18 reveals an overlap distance of $d/D \approx 0.25$ at which both the predicted and measured noise radiation from the propeller is a maximum at this frequency, which generally dominates the overall sound power level, as shown in Figure 3. It is evident that the maximum noise scenario occurs when the propeller overlaps 50% with the wing. This has previously been observed for overlapping contra-rotating propellers with offset, where a partial 50% overlap produces the highest noise levels [28].

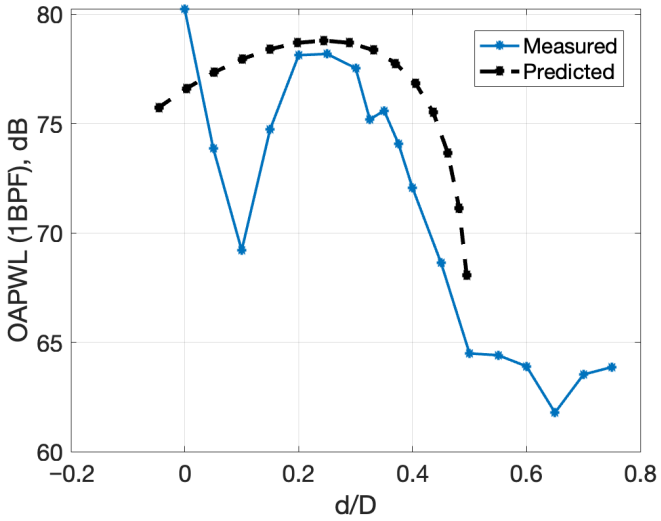

Figure 18. Predicted overall sound power level at 1 BPF plotted against overlap distance d/D. The mean thrust per blade is set to 5 N, given that the total thrust generated by the propeller is 10 N.

Whilst the simple model is able to capture the general behaviour of the noise variation with d/D it is unable to predict its detailed variations, such as the dip in noise at $d/D = 0.1$ due to the presence of additional noise sources, their relative balance and the ground reflections addressed in Section 4.4.1. This broad level of agreement provides some evidence that the dominant noise-generating mechanism at takeoff for close separation distances is the unsteady loading of the propeller.

It is noteworthy that for lower values of separation distances $z/D < 0.2$, the effect of mean flow distortion also contributes to generating unsteady loading on the propellers due to high blockage effects from the wing. Given the complexity of the problem, in this study, we follow the analysis based on [23], where the velocity harmonics required in the noise

calculation are deduced from the measured hot-wire data from the plane upstream of the propeller. This analysis will be presented in detail in Section 4.4.3.

4.4.3. Role of Inflow Distortion

Another significant additional noise source that arises in the presence of a wing in close proximity to a propeller is the inflow distortion noise onto the propeller induced by the wing. The non-uniform mean flow and turbulence caused by the inflow distortion can result in unsteady loading on the propeller blades. In this section, inflow hot-wire velocity data obtained from Figure 10 is used as input to predict the noise generated by the propeller due to inflow distortion induced by the wing based on the propeller noise model due to inflow distortion presented by Xie et al. [23].

The model, based on flat plate theory, uses as input the velocity amplitudes U_n of the inflow harmonics at each radial position, which were deduced from the azimuthal variation in hot-wire velocity measurements from $U_n = \int (U(\theta) \cos(n\theta) d\theta$. The far-field acoustic pressure is predicted from U_n using the methodology outlined by [23]. This approach only predicts the tonal component due to unsteady loading noise due to inflow distortion. However, the inflow turbulence-propeller interactions are ignored in this analysis. A key assumption of our model is that the blades are relatively thin, where our blade thicknesses vary between 4–8%. Based on our previous numerical work [29], flat-plate response models show excellent agreement with airfoil responses at these thickness levels. Moreover, the inflow variation due to wing blockage is approximately 8 m/s, which is small compared to the propeller tip speed of 80 m/s, corresponding to a change in angle of attack of only about 5.5°. No other simplifications are introduced in the model. We hope this explanation is satisfactory.

The predicted tonal spectra with and without wing are presented in Figure 19a and compared against the measured data shown in Figure 19b. Both measurement and prediction indicate an increase in noise by between 2 and 3 dB due to flow distortion, although predictions slightly exceed measurements. The biggest discrepancy between prediction and measurement is observed at the first blade passing frequency (1 BPF), where measurements indicate a 15 dB increase noise at 1 BPF compared with less than 1 dB obtained from prediction.

This increase in measured noise therefore cannot be solely attributed to inflow distortion and other mechanisms must be present not included in the model, such as unsteady loading due to 'ground effects' and potential field interactions. High fidelity computations are therefore necessary to compare against other potential interaction sources and validate the results with experimental data.

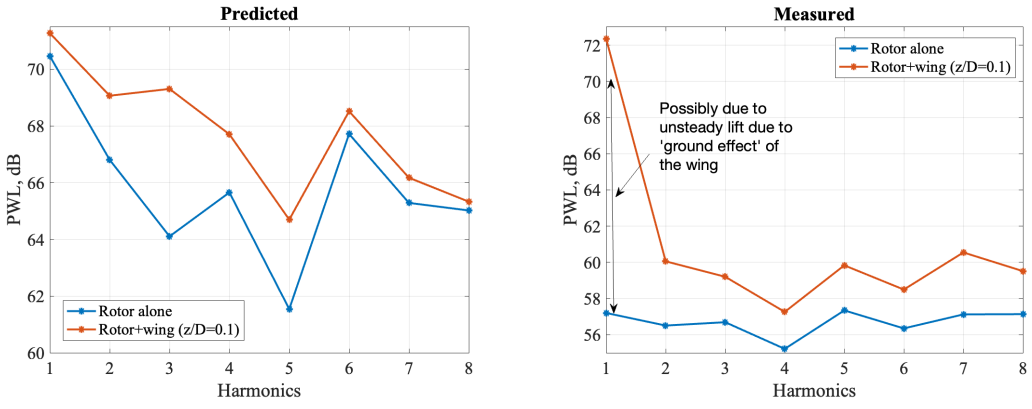

(**a**) Analytical predictions. (**b**) Measured data for tonal noise harmonics.

Figure 19. Analytical (**a**) and experimental (**b**) evidence for the role of inflow distortion in tonal noise harmonics for a wing placed at $z/D = 0.1$ and $d/D = 0.25$.

4.4.4. Role of Potential Field Interactions

When the propeller operates in close proximity to the wing, one of the dominant sources of interaction noise is potential field interactions [6], arising from a non-axisymmetric upwash velocity on the propeller due to the potential field of the wing. We hypothesised this noise source to be dominant at a separation distance of $z/D = 0.1$ and smaller overlap distances $d/D < 0.1$, as depicted in Figures 3 and 6a. Similarly, the bound potential field of the propeller also radiates noise as it rotates past the wing leading edge and scatters into sound. For conventional propeller–wing configurations during cruise, analytical models are available that describe the dominant potential-field interaction mechanisms [6,24]. However, for the configuration considered in this study, the individual contributions from the two potential-field interaction noise mechanisms are not known and remain to be determined.

4.5. Interpretation: Radiation from Wing

This study has demonstrated that propeller noise is a dominant noise source during takeoff compared to wing interaction noise sources. However, the wing may also play a significant role, particularly when flow velocities impacting the wing are relatively high. In this section, we present various possible wing interaction noise sources present in this propeller configuration at takeoff.

4.5.1. Edge Scattering by the Wing by Wake/Tip Vortex Flow

Figure 20 presents a sketch of the source mechanisms involving the unsteady flow generated by the propeller interacting with the wing during takeoff. In this study, we have qualitatively identified the primary region on the wing where the tip vortex interacts, as the tip vortex represents a dominant coherent structure compared to the conventional wake. Predicting the aerodynamic and acoustic behaviour in this scenario is particularly challenging because, during takeoff, the unsteady flow impinges perpendicularly on the wing, as shown in Figure 20. Classical Sears-type blade response functions fail in this case, as the flow becomes highly separated from the wing. High-fidelity computational fluid dynamics (CFD) simulations are therefore essential to establish the relationship between the unsteady flow striking the wing, the resulting unsteady surface pressure response, and the subsequent far-field noise radiation.

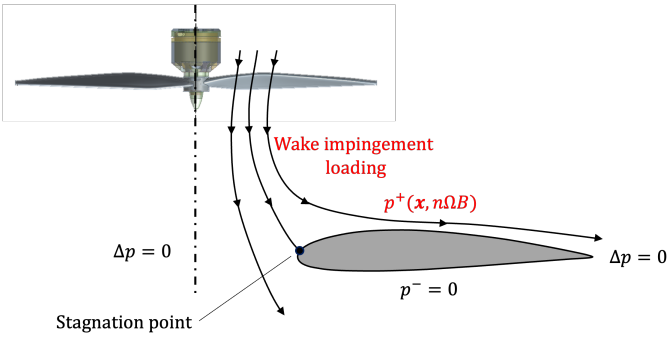

Figure 20. Source mechanism schematic of unsteady flow when propeller is interacting wing.

4.5.2. Edge Scattering by the Wing by Rotor Potential Field

Another potentially important source of noise, particularly at small separation distances ($z/D < 0.1$), is due to the interaction between the bound potential field of the rotor interacting with the wing. Evidence for the presence of potential field interaction can be observed in Figures 3 and 6a especially for $d/D < 0.1$. As the offset increases, the overall noise level at the first blade passing frequency (1 BPF) decreases rapidly, consistent with

the predictions made by Akiwate and Parry [30]. Although their formulation is related to an in-flight propeller–wing configuration, a similar interaction mechanism is likely to occur in our specific takeoff configuration when the wing is perpendicular to the propeller flow. Further research is needed to develop models that accurately capture the potential interaction between the propeller and wing during takeoff conditions.

4.5.3. Leading Edge Separation

In addition to the noise due to leading edge scattering, another potential noise source arises from the presence of separated flow occurring at the wing leading edge. However, in the context of the current study, where flow velocities are relatively low, this source is likely to be comparatively minor compared to other sources. Nevertheless, in practical scenarios where flow velocities impacting the wing are higher, separation noise may become significant, particularly at lower frequencies. Further research is required to explore this noise source, especially when the flow impacts the wing perpendicularly to the wing plane (takeoff configuration).

5. Conclusions

This paper has examined the noise generation mechanisms of a fixed-wing VTOL configuration in a takeoff hover condition, focusing on how propeller–wing proximity influences the radiated sound. Acoustic measurements, hot-wire velocity data, and analytical modelling were used to study the effects of vertical separation (z/D) and horizontal offset or overlap (d/D).

The results confirm that the dominant mechanism is the unsteady loading induced on the propeller by the presence of the wing, particularly at small separation distances where tonal levels increase due to ground-effect-type interactions. The study also shows that the maximum noise occurs when the propeller overlaps the wing by approximately 50%, a trend consistent with previous observations for overlapping contra-rotating propellers with offset. Additionally, when the propeller and wing overlap, the wing also acts as an effective image source, creating constructive and destructive interference patterns evident in the broadband spectra. Although the wing has a measurable influence, its direct noise contribution is significantly weaker than that of the propeller. The findings also show that analytical models developed for conventional cruise configurations are not directly applicable to the tilted and overlapping architectures considered here, highlighting a need for more suitable modelling approaches.

Overall, the study provides new physical insight into how propeller–wing proximity modifies the radiated sound through a combination of unsteady loading, interference effects, and flow distortion. While some mechanisms remain tightly coupled and require high-fidelity simulations for full separation, the present results clearly identify propeller-driven mechanisms as the dominant contributors. The wing nevertheless influences the acoustic field by inducing unsteady loads and by acting as an image source in overlapping arrangements. These observations provide guidance for designing low-noise fixed-wing VTOL vehicles and for developing effective noise-abatement strategies for urban air mobility and unmanned aircraft systems.

Author Contributions: Conceptualisation, P.C. and S.P.-C.; methodology, P.C.; validation, P.C., P.J. and S.P.-C.; formal analysis, P.C.; investigation, T.C., S.P.-C., M.C., A.K., P.J., D.C.A., O.W. and S.K.; writing—original draft preparation, P.C.; writing—review and editing, S.P.-C., P.J., D.C.A., O.W. and S.K.; supervision, P.C.; funding acquisition, P.C. All authors have read and agreed to the published version of the manuscript.

Funding: The first author would like to acknowledge the financial support of the Royal Academy of Engineering (RF\201819\18\194).

Data Availability Statement: The original contributions presented in the study are included in the article, further inquiries can be directed to the corresponding author.

Acknowledgments: The authors would also like to thank Rolls-Royce for technical support. Deepak Akiwate gratefully acknowledges the support of a University Fellowship from the University of Salford.

Conflicts of Interest: The authors declare no conflicts of interest.

References

1. Mann, S.; Stuart, C. Advanced propulsion through the 1990s-An airframer's view. In Proceedings of the 21st Joint Propulsion Conference, Monterey, CA, USA, 8–11 July 1985; p. 1192. [CrossRef]
2. Parry, A.B. Theoretical Prediction of Counter-Rotating Propeller Noise. Ph.D. Thesis, University of Leeds, Leeds, UK, 1988.
3. Akkermans, R.A.; Pott-Pollenske, M.; Buchholz, H.; Delfs, J.; Almoneit, D. Installation effects of a propeller mounted on a high-lift wing with a Coanda flap. Part I: Aeroacoustic experiments. In Proceedings of the 20th AIAA/CEAS Aeroacoustics Conference, Atlanta, GA, USA, 16–20 June 2014; p. 3191. [CrossRef]
4. Sinnige, T. Aerodynamic and Aeroacoustic Interaction Effects for Tip-Mounted Propellers: An Experimental Study. Ph.D. Thesis, Delft University of Technology, Delft, The Netherlands, 2018.
5. Zawodny, N.S.; Boyd, D.D.; Nark, D.M. Aerodynamic and Acoustic Interactions Associated with Inboard Propeller-Wing Configurations. In Proceedings of the AIAA Scitech 2021 Forum, Virtual, 11–15 & 19–21 January 2021; p. 0714. [CrossRef]
6. Chaitanya, P.; Akiwate, D.C.; Palleja-Cabre, S.; Karimian, A.; Joseph, P.; Parry, A.B. Investigation into the mechanisms of propeller-wing interaction noise. In Proceedings of the 28th AIAA/CEAS Aeroacoustics 2022 Conference, Southampton, UK, 14–17 June 2022. [CrossRef]
7. Silva, C.; Johnson, W.; Antcliff, K.R.; Patterson, M.D. VTOL urban air mobility concept vehicles for technology development. In Proceedings of the 2018 Aviation Technology, Integration, and Operations Conference, Atlanta, GA, USA, 25–29 June 2018; pp. 1–16. [CrossRef]
8. Lee, T.; Leishman, J.; Manikandan, R. Fluid Dynamics of Interacting Blade Tip Vortices with a Ground Plane. *J. Am. Helocopter Soc.* **2010**, *55*, 22005. [CrossRef]
9. Hanson, L.; Jawahar, H.K.; Vemuri, S.S.; Azarpeyvand, M. Experimental investigation of propeller noise in ground effect. *J. Sound Vib.* **2023**, *559*, 117751. [CrossRef]
10. Hanson, D.B. Noise of counter-rotation propellers. *J. Aircr.* **1985**, *22*, 609–617. [CrossRef]
11. Magliozzi, B.; Hanson, D.; Amiet, R. Propeller and propfan noise. *Aeroacoustics Flight Veh. Theory Pract.* **1991**, *1*, 1–64.
12. Node-Langlois, T.; Wlassow, F.; Languille, V.; Colin, Y.; Caruelle, B.; Gill, J.R.; Chen, X.; Zhang, X.; Parry, A.B. Prediction of contra-rotating open rotor broadband noise in isolated and installed configurations. In Proceedings of the 20th AIAA/CEAS Aeroacoustics Conference, Atlanta, GA, USA, 16–20 June 2014; p. 2610. [CrossRef]
13. Roger, M.; Schram, C.; Moreau, S. On vortex-airfoil interaction noise including span-end effects, with application to open-rotor aeroacoustics. *J. Sound Vib.* **2014**, *333*, 283–306. [CrossRef]
14. Ekoule, C.M. Advanced Open Rotor Far-Field Tone Noise. Ph.D. Thesis, University of Southampton, Southampton, UK, 2017.
15. Quaglia, M.E.; Léonard, T.; Moreau, S.; Roger, M. A 3D analytical model for orthogonal blade-vortex interaction noise. *J. Sound Vib.* **2017**, *399*, 104–123. [CrossRef]
16. Acevedo-Giraldo, D.; Roger, M.; Jacob, M.C.; Bériot, H. Analytical study of the aerodynamic noise emitted by distributed electric propulsion systems. In Proceedings of the 28th AIAA/CEAS Aeroacoustics 2022 Conference, Southampton, UK, 14–17 June 2022. [CrossRef]
17. Roger, M.; Acevedo-Giraldo, D.; Jacob, M.C. Acoustic versus aerodynamic installation effects on a generic propeller-driven flying architecture. *Int. J. Aeroacoustics* **2022**, *21*, 585–609. [CrossRef]
18. Chen, M.; Liu, L.; Chen, Y. Aeroacoustic and aerodynamic measurements at the rotor plane in the interaction of a small rotor with wings. *J. Acoust. Soc. Am.* **2024**, *156*, 2816–2828. [CrossRef] [PubMed]
19. Chen, M.; Chen, Y.; Hua, J.; Maier, N.; Burdette, D. Experimental assessment of blowing effect on vehicle performance and aero-acoustics in small-rotor/wing interaction. *J. Vib. Control* **2025**, *31*, 966–980. [CrossRef]
20. Chen, M.; Liu, T.; Wimsatt, J.; Edwards, J. Numerical Study of a Small Rotor Interacting with a Generic Wing Using a Transient Solver. In Proceedings of the AIAA Aviation Forum and ASCEND, Las Vegas, NV, USA, 21–25 July 2025. [CrossRef]

21. Chaitanya, P.; Cho, M.; Palleja-Cabre, S.; Akiwate, D.C.; Joseph, P.; Westcott, O.; Ferraro, M. Aeroacoustics source mechanisms of fixed-wing VTOL configuration. In Proceedings of the AIAA AVIATION 2023 Forum, San Diego, CA, USA, 12–16 June 2023. [CrossRef]
22. Cai, J.; Gunasekaran, S.; Ol, M. Effect of Partial Ground and Partial Ceiling on Propeller Performance. *J. Aircr.* **2023**, *60*, 648–661. [CrossRef]
23. Xie, J.; Zhou, Q.; Joseph, P.F. Tone Noise Prediction of a Propeller Operating in Nonuniform Flows. *AIAA J.* **2011**, *49*, 111–118. [CrossRef]
24. Akiwate, D.C.; Parry, A.B.; Joseph, P.; Paruchuri, C.C. Analytical investigation of propeller-wing interaction noise. In Proceedings of the 28th AIAA/CEAS Aeroacoustics Conference, Southampton, UK, 14–17 June 2022. [CrossRef]
25. Amiet, R.K. High frequency thin-airfoil theory for subsonic flow. *AIAA J.* **1976**, *14*, 1076–1082. [CrossRef]
26. Ingard, U.; Lamb, G.L. Effect of a Reflecting Plane on the Power Output of Sound Sources. *J. Acoust. Soc. Am.* **1957**, *29*, 743–744. [CrossRef]
27. Goldstein, M. *Aeroacoustics*; McGraw-Hill International Book Co.: New York, NY, USA, 1976.
28. Paruchuri, C.C.; Joseph, P.; Akiwate, D.C.; Parry, A.B.; Prior, S.D. On the noise generation mechanisms of overlapping propellers. In Proceedings of the AIAA Aviation 2021 Forum, Virtual, 2–6 August 2021; p. 2281. [CrossRef]
29. Gill, J.; Zhang, X.; Joseph, P. Symmetric Airfoil Geometry Effects on Leading Edge Noise. *J. Acoust. Soc. Am.* **2013**, *134*, 2669–2680. [CrossRef] [PubMed]
30. Akiwate, D.C.; Parry, A.B. Propeller wake interaction noise with downstream wing: Effect of wing sweep, lean, and offset. In Proceedings of the AIAA Aviation 2023 Forum, San Diego, CA, USA, 12–16 June 2023. [CrossRef]